

Elucidation of C₂ and CN formation mechanisms in laser-induced plasmas through correlation analysis of carbon isotopic ratio

Meirong Dong^{a,b}, George C.-Y. Chan^b, Xianglei Mao^b, Jhanis J. Gonzalez^b, Jidong Lu^a, Richard E. Russo^{b*}

^a*School of Electric Power, South China University of Technology, Guangzhou, Guangdong, 510640, China*

^b*Lawrence Berkeley National Laboratory, Berkeley, CA 94720, USA*

*Corresponding Author: Richard E. Russo (RERusso@lbl.gov)

Abstract

Laser Ablation Molecular Isotopic Spectrometry (LAMIS) was recently reported for rapid isotopic analysis by measuring molecular emission from laser-induced plasmas at atmospheric pressure. With ¹³C-labelled benzoic acid as a model sample, this research utilized the LAMIS approach to clarify the formation mechanisms of C₂ and CN molecules during laser ablation of organic materials. Because the isotopic ratios in the molecular bands could deviate from statistical distribution depending on their formation pathways, the dominant mechanism can be identified through a comparison of the experimental observed isotopic patterns in the molecular emission with the theoretical statistical pattern. For C₂ formation, the experimental ¹²C¹²C / ¹³C¹²C ratios support a recombination mechanism through atomic carbon at early delay time but also indicate the presence of other operating mechanisms as the plasma evolves; it is proposed that some of the C₂ molecules are released directly from the aromatic ring of the sample as molecular fragments. In contrast, the temporal profiles in the ¹²C / ¹³C ratios derived from CN emission exhibited opposite behavior with those derived from C₂ emission, which unambiguously refutes mechanisms that require C₂ as a precursor for CN formation; CN formation likely involves atomic carbon or species with a single carbon atom.

1 Introduction

When a high-powered pulsed laser is focused onto a sample surface, a plasma is formed. This laser-induced plasma contains atomic, molecular, and cluster-like chemical species, which are either ablated directly from the irradiated target or produced through gaseous-phase chemical reactions in the plasma [1]. The chemical content of the sample can be interrogated by optical emission spectrometry from this plasma. For example, laser-induced breakdown spectroscopy (LIBS), which measures atomic emission, offers almost ideal characteristic for real-time elemental analysis at atmospheric pressure [2-6]. Molecular spectral signatures also provide valuable chemical information of the sample. Particularly relevant to the present study is the importance of C_2 and CN molecular emission for classification of organic materials.

Sattmann *et al.* [7] derived a scheme to identify polymers based on C_2 emission and C/H atomic-emission ratios. Grégoire *et al.* [8] reported that C_2 molecular emission is crucial in improving the accuracy of polymer classification. Anzano *et al.* [9] employed C_2 and CN bands, atomic carbon, hydrogen, oxygen and nitrogen emission intensity ratios to classify polymeric materials, and reported that C_2/C and H/C are the two most important ratios. Material classification with LIBS molecular signatures is not limited only to synthetic polymers. Through direct ablation of the native CN bonds from bacterium, Baudelet *et al.* [10] demonstrated the detection and identification of *Escherichia coli* with LIBS from the strong CN molecular emission. Lucena *et al.* [11] utilized atomic, ionic and molecular emission of different species in the plasma to distinguish explosives that are composed of different classes of organic compounds, and concluded that molecular emission constitutes an important source of information for identification purposes.

The optical emission also provides a powerful tool for *in-situ* plasma diagnosis. For example, Parigger *et al.* [12] reported the use of atomic and molecular carbon emission as diagnostic tools to study nanoparticles production in a laser plasma. Acquaviva *et al.* [13, 14] studied temporal- and spatial-resolved optical emission of C₂ and CN generated during laser ablation of graphite in order to use the molecular information for thin film deposition. Dinescu *et al.* [15] demonstrated that C₂ and CN band intensities are strong functions of laser fluence, N₂ pressure, and position in the plasma plume during laser ablation of graphite in a nitrogen environment. Molecular information also can be used to correct for plasma fluctuations, as presented in our previous work [16].

Clearly, C₂ and CN are important and widely adopted molecules for both analytical applications and plasma diagnostics; yet, their formation mechanisms in the laser-induced plasma are still not fully understood and are subjects of debate. Several processes, such as the laser material interaction, plasma formation, plasma expansion, and collisional excitation of atoms in the plume have been investigated in detail by various research groups [17-21]. Kinetic modellings for molecular formation in laser plasmas [22, 23] also has been developed, but the formation mechanisms for the C₂ and CN molecules remain controversial. Two reaction pathways have been proposed for the formation of CN molecules in laser plasmas – one comprises molecular C₂ as the precursor [23-26] whereas the other one involves atomic C [15, 22, 23, 26, 27], which reacts either directly with N₂ molecules [23, 26, 27] in air or atomic nitrogen [15, 26]. So far, it is not well established which reaction pathway is dominant. The objective of the present study is to clarify the mechanisms leading to the formation of C₂ and CN molecules during laser ablation

of an organic compound in ambient air, through the use of isotope labelling and laser ablation molecular isotopic spectrometry (LAMIS).

The LAMIS technique is implemented similar to conventional LIBS elemental analysis but measures molecular emission in the laser-induced plasma, and gives isotopic information of the sample in a real-time fashion under ambient environment [28-35]. The advantage of LAMIS over LIBS for isotopic analysis is that isotope shifts in molecular spectra are orders of magnitude larger than those in atomic spectra, due to the appreciable effect of different isotopic masses on the vibrational and rotational energy levels in molecules, compared to small effects on electronic transitions (atoms) [28]. Therefore, it is possible to determine isotopes at atmospheric pressure with a relatively small optical spectrometer through measurement of molecular emission. Previous published LAMIS works include isotopes from carbon, hydrogen, boron and strontium [28-35]. In addition, LAMIS also can be employed to study molecular formation in laser-induced plasma [33].

In this work, spatial and temporal features for C₂ and CN molecular emission from ablation of benzoic acid with ¹³C labelling were measured. Only the terminal carbon atom (i.e., the one in the carboxylic-acid group) is isotopically labelled and the six carbon atoms in the aromatic ring preserve natural isotopic abundance. Therefore, the ¹²C / ¹³C ratio in the sample is approximately 6 : 1. As will be discussed, the isotopic ratios in the molecular bands could deviate from the statistical distribution, depending on their reaction pathways. Therefore, through an analysis of the ¹²C / ¹³C isotopic ratios derived from the corresponding molecular

bands, the dominant mechanisms for C₂ and CN formation in laser-induced plasma can be identified.

2 Experimental

2.1 Experimental

With the exception of the laser pulse energy and the magnification ratio of the imaging system, the temporal- and spatial-resolved optical emission monitoring system is identical to the one previously described [33]. Briefly, a nanosecond Q-switched Nd:YAG laser operated at 1064 nm, with 100 mJ pulse energy, was focused with a fused-silica lens to a spot diameter of ~ 250 μm onto the sample surface to generate the plasma. The laser-induced plasma was imaged by two fused-silica lenses onto a linear array fiber bundle (4.9 mm high × 0.245 mm wide), with a 200 μm core diameter for each fiber. The ratio of the plasma-to-fiber distance was ~ 1:1.3. The other end of the fiber bundle was imaged by a lens onto the entrance slit of a Czerny-Turner spectrometer (Horiba JY 1250M), coupled with an intensified-CCD (ICCD) detector. Individual fibers in the array can be distinguished in the ICCD image, and each fiber (0.245 mm) corresponded to ~ 0.188 mm height in the plasma.

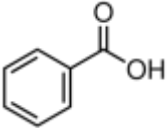
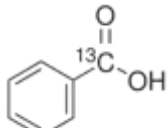
The emission evolution of two molecular (C₂ and CN) and four atomic (C, H, O and N) species was studied as these species represent native characteristics for a large variety of organic compounds. The spectrometer was equipped with changeable gratings and two gratings were used, depending on the measured wavelengths and the required spectral resolution. For the C, CN and C₂ emission in the wavelength region between 200 and 500 nm, a 3600 grooves mm⁻¹ grating with a spectral resolution of 0.01 nm was used. For H, O and N emission between 600

and 800 nm, a 1200 grooves mm^{-1} grating with 0.04 nm spectral resolution was sufficient. Temporal profiles of the emission were recorded by varying the gate delay of the ICCD detector with respect to the laser pulse. The ICCD gate width also was varied according to the gate delay, but the ratio of the gate width to gate delay was fixed at 0.75.

2.2 Samples

Benzoic acid samples with natural carbon-isotope abundance and ^{13}C labelling were used; the only ^{13}C -labelled site was at the terminal carboxylic acid group. The molecular formula and chemical structure for the two samples (both obtained from Sigma-Aldrich Corporation) are shown in Table 1. The powder samples were pressed with 7 tons of force for 4 min into a one-centimeter diameter pellet. The samples were ablated with 40 laser shots per sampling location, and one spectrum per location was obtained by setting the ICCD to accumulation mode. This procedure was repeated on four locations for each sample. The measurements were performed in air at atmospheric pressure. The ablated material was exhausted to a hood through a filter.

Table 1 Chemical formula and structure of samples studied in this work.

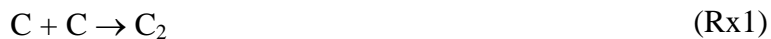
Chemical	Formula	Structure	Characteristic
Benzoic acid (^{12}C)	$\text{C}_6\text{H}_5\text{CO}_2\text{H}$		Purity $\geq 99.5\%$; 68.85 wt.% C
Benzoic acid- α - ^{13}C ($^{12}\text{C} : ^{13}\text{C} = 6 : 1$)	$\text{C}_6\text{H}_5^{13}\text{CO}_2\text{H}$		^{13}C -labelled terminus (99% ^{13}C purity); 69.11 wt.% C

3 Results and Discussion

3.1 Link between reaction mechanisms and isotopic patterns in C₂ and CN emission

The ¹³C-labelled benzoic acid sample was used for elucidation of C₂ and CN formation mechanisms in laser-induced plasma under ambient environment. As will be discussed below, the isotopic patterns in C₂ and CN emission could change according to their reaction pathways. Therefore, the importance of a candidate mechanism can be assessed by a comparison of the experimental observed patterns in the molecular emission with the theoretical pattern based on pure statistical analysis. First, let us assume that all the carbon atoms in the benzoic acid have equal probability to be dissociated into atomic carbon (i.e., there is no preferential bond breakage) in the energetic laser plasma, and let R be the ratio of ¹²C / ¹³C in the sample (i.e., $R = 6$ in the ¹³C-labelled benzoic acid employed in the present study).

A candidate reaction for C₂ molecular formation is through recombination of carbon atoms:



Under Rx1, the anticipated number densities of ¹²C¹²C : ¹³C¹²C : ¹³C¹³C, based on statistical distribution, should be $R^2 : 2R : 1$ [36-38] (i.e., 36 : 12 : 1 for the ¹³C-labelled benzoic acid). If the observed isotopic patterns in the C₂ emission do not follow this ratio, then either Rx1 is not the dominant mechanism for C₂ formation or the main assumption that there is no preferential bond dissociation of the sample is not valid. For example, if the plasma is not energetic to atomize all the chemical bonds of the ablated materials, those molecular fragments that originate directly from the sample preserve their chemical-bond arrangements as in the solid sample. If the sample contains an isotopically enriched site, such chemical-bond information will then be coded in the isotope ratio of the molecular fragments. It has been proposed that C₂ molecules

can be directly released from the sample as fragments, without undergoing atomization, during laser sampling [8, 25, 33, 39]. Under this direct C₂-release hypothesis, the emission pattern of ¹²C¹²C : ¹³C¹²C : ¹³C¹³C could deviate from the statistical $R^2 : 2R : 1$ ratio.

If the sample contains no nitrogen (as in the case of benzoic acid), CN molecules must be formed through chemical reactions between some C-containing species with nitrogen in air, either directly with N₂ molecules or with N atoms. In these experiments, it is not possible to distinguish which N-species is more significant for CN formation; however, the identity of the C-species that is more important can be clarified. Both atomic carbon (Rx2a and Rx2b) and molecular C₂ (Rx3a and Rx3b) are the two widely discussed precursors for the formation of CN radicals, through reactions:



Based purely on statistical arguments, the isotopic patterns in CN emission are identical for these two precursors. For Rx2a and Rx2b, the ratio of ¹²CN : ¹³CN is $R : 1$ (i.e., 6 : 1 for the ¹³C-labelled benzoic acid). If Rx1 is the sole mechanism for C₂ formation, which gives ratios $R^2 : 2R : 1$ for ¹²C¹²C : ¹³C¹²C : ¹³C¹³C, and because each C₂ molecule can produce 2 CN molecules, the expected ratio of ¹²CN : ¹³CN should follow $(2R^2 + 2R) : (2R + 2)$, which simplifies to $R : 1$. Therefore, if there is no preference in bond dissociation of the sample (i.e., all carbon atoms in the benzoic acid have identical probability to be atomized by the laser-induced plasma), and no conclusion can be drawn on the CN-formation mechanism. However, if

the isotopic patterns in C₂ molecules deviate from the statistical distribution due to contributions from other mechanisms (e.g., direct C₂-release), the importance of C₂ as a precursor for CN can be assessed through a correlation analysis of the isotopic patterns in ¹²CN : ¹³CN and ¹²C¹²C : ¹³C¹²C ratios.

3.2 Isotopic analysis from C₂ and CN molecular emission

The rotational and vibrational energy levels of a molecule are changed, upon replacement of an atom by its isotope. As a result, the emission wavelengths are altered and this isotopic shift allows the fractions of C₂ and CN molecules that are made up from different carbon isotopes to be determined from the corresponding molecular spectra. The C₂ Swan band $d^3\Pi_g - a^3\Pi_g$ (1-0) and CN violet band $B^2\Sigma^+ - X^2\Sigma^+$ (0-1) were chosen in this study because these two bands have strong intensity and appreciable isotopic shifts.

Similar to our previous study [16], the analytical information is extracted by fitting the experimental emission spectra with synthetic spectra [40-42]. The algorithm is similar to previously reported [33], except that a few changes have been implemented to improve the fitting. First, instead of calculating all the theoretical rotational-line positions through the vibrational and rotational constants of the molecules, experimentally reported rotational structures [43-46] are used throughout whenever available. The recent compilations of C₂ and CN rotational structures by Brooke *et al.* [43] and Ram *et al.* [44], respectively, are particularly useful. The use of experimentally determined rotational structure takes into account slight wavelength shifts of some rotational components due to perturbations; several studies reported that many rotational levels in the $d^3\Pi_g$ $v = 0-2$ state of C₂ (i.e., the measured C₂ Swan band in

the current study) are perturbed by other electronic states [47]. Second, unlike in our previous work, we intentionally omitted the fitting of $^{13}\text{C}^{13}\text{C}$ in this study because this band was weak due to the low abundance of ^{13}C in the labelled sample; only $^{12}\text{C}^{12}\text{C}$ and $^{13}\text{C}^{12}\text{C}$ were used in fitting the C_2 spectrum. Figure 1 shows a spectrum of the C_2 $d^3\Pi_g - a^3\Pi_g$ (1–0) band from the ^{13}C -labelled benzoic acid, the $^{12}\text{C}^{12}\text{C}$ and $^{13}\text{C}^{12}\text{C}$ bands were strong and readily identified; however, the $^{13}\text{C}^{13}\text{C}$ band was weak and barely distinguishable from the baseline noise. As discussed in the last section, the expected strength of the $^{13}\text{C}^{13}\text{C}$ band is weaker than the $^{13}\text{C}^{12}\text{C}$ band by a factor of 12, and these three C_2 bands from different isotopes are well separated in wavelength (i.e., only the tail of the $^{13}\text{C}^{13}\text{C}$ band enters the $^{13}\text{C}^{12}\text{C}$ spectral region, cf. Figure 1). Because the $^{13}\text{C}^{13}\text{C}$ band was noisy, a fitting algorithm including the $^{13}\text{C}^{13}\text{C}$ band could indeed degrade the overall accuracy. Therefore, the $^{13}\text{C}^{13}\text{C}$ band was excluded in the fitting.

A set of theoretical spectra for $^{12}\text{C}^{12}\text{C}$ and $^{13}\text{C}^{12}\text{C}$ (denoted as $I_{12\text{C}^{12}\text{C}}^{\text{syn}}(\lambda, T_{\text{rot}})$ and $I_{13\text{C}^{12}\text{C}}^{\text{syn}}(\lambda, T_{\text{rot}})$ respectively) were generated with experimental reported wavelengths (λ) [43, 45], whenever available, for each rotational component in the C_2 $d^3\Pi_g - a^3\Pi_g$ (1–0) band. Intensity distribution of each rotational component is calculated based on rotational line strengths (i.e., the Hönl–London factors) and the Boltzmann distribution under a certain rotational temperature (T_{rot}). Because the spectrum contained only one vibrational band, the Franck–Condon coefficient was not needed in the present fitting. The most relevant fitting parameters are rotational temperature (T_{rot}), continuum background ($I_{\text{continuum}}$), relative number densities of $^{12}\text{C}^{12}\text{C}$ and $^{13}\text{C}^{12}\text{C}$ in the $d^3\Pi_g$ ($v = 1$) state (denoted as α_{C_2} and β_{C_2} , respectively). The fitting algorithm locates the best combination of all fitting parameters by minimization of the sum of

the squares of the fitting residuals ($\epsilon(\lambda)$) at all wavelengths (λ) of the experimental spectrum, $I_{C_2}^{expt}(\lambda)$, through

$$I_{C_2}^{expt}(\lambda) = [\alpha_{C_2} \times I_{^{12}C^{12}C}^{syn}(\lambda, T_{rot}) + \beta_{C_2} \times I_{^{13}C^{12}C}^{syn}(\lambda, T_{rot})] + I_{continuum} + \epsilon(\lambda)$$

A similar procedure was used for fitting the CN $B \ ^2\Sigma^+ - X \ ^2\Sigma^+$ (0–1) band; a set of theoretical spectra for $^{12}C^{14}N$ and $^{13}C^{14}N$ (denoted as $I_{^{12}CN}^{syn}(\lambda, T_{rot})$ and $I_{^{13}CN}^{syn}(\lambda, T_{rot})$ respectively) were generated with experimentally determined rotational structures [44, 46], and the fitting algorithm locates the relative number densities of $^{12}C^{14}N$ and $^{13}C^{14}N$ in the $B \ ^2\Sigma^+$ ($v = 0$) state (denoted as α_{CN} and β_{CN} , respectively) from the experimental spectra, $I_{CN}^{expt}(\lambda)$, through

$$I_{CN}^{expt}(\lambda) = [\alpha_{CN} \times I_{^{12}CN}^{syn}(\lambda, T_{rot}) + \beta_{CN} \times I_{^{13}CN}^{syn}(\lambda, T_{rot})] + I_{continuum} + \epsilon(\lambda)$$

The quality of the fitting is further gauged by the relative residual, which is defined as

$$\text{Rel. Residual} = \frac{\sum |I^{expt} - I^{syn}|}{\sum |I^{expt} - I_{continuum}|}$$

The physical meaning of the relative residual can be regarded as the relative error of the area under the experimental and fitted spectral profiles. To focus on the fitting quality of only molecular emission, $I_{continuum}$ is subtracted from I^{expt} in the dominator. A wide range of relative residuals from ~ 0.15 to > 0.70 was obtained, depending on the signal-to-noise ratio of the molecular emission. Visual inspections of the fittings (cf. Figures 2a and 2b) reveal that the fitting can be classified as good for its intended purpose when relative residual is less than 0.20. When the relative residual increases to ~ 0.35 , the fitting becomes marginal but still acceptable. The fitting quality further degrades for higher relative residuals. To demonstrate the quality of fitting, two spectra for C_2 with relative residuals 0.164 (i.e., a good fit) and 0.356 (i.e., close to

threshold) are presented in Figure 2a. Figure 2b gives a set of similar spectra for CN. Although somewhat subjective, relative residual 0.35 was chosen as a threshold, and we report only those results with relative residuals lower than this threshold. Averaging multiple spectra from the same experiment enhances signal-to-noise ratio and improves the fitting quality. For each studied ICCD delay time, four sets of spectra were measured. In cases that the relative residuals of individual spectra at some spatial locations were greater than the threshold, those four spectra were averaged with fitting subsequently performed. If the relative residual of the averaged spectra was lower than the threshold, then results from the averaged spectra were used for those spatial locations. This arrangement allows data continuity in the spatial profiles as complete as possible while maintaining a high standard of spectral fitting. Of course, the drawback of averaging is a lack of estimation for the measurement uncertainty (i.e., no error bar).

3.3 Spatial emission and plasma-temperature profiles from natural and isotope-labelled benzoic acid

Before evaluation of isotopic patterns in the C₂ and CN molecular bands from the ¹³C-labelled benzoic acid and elucidation of reaction pathways, it is important to first establish if this isotopic substitution influenced properties of the laser induced plasma. Any molecular formation mechanism derived from the ¹³C-labelled sample can be extended to “normal” samples (i.e., those with natural isotopic abundance) only when the plasma conditions between the two samples are similar. After all, chemical reactions are strong functions of reactant concentrations (in the present study, particularly densities of gaseous atoms), temperature, and electron density. Therefore, plasma properties from ablation of benzoic acid samples with natural isotope abundance and ¹³C-labelled terminus were compared. The plasma characteristics include spatial-

and temporal-resolved profiles of atomic and molecular emission, rotational temperatures, and linewidth of H_{α} emission line, which reflects the electron number density of the plasma.

Profiles of atomic (C I 247.8 nm, H I 656.3 nm, O I 777.4 nm and N I 746.8 nm) and molecular (C_2 Swan band, $d^3\Pi_g - a^3\Pi_g$ (1-0), and CN violet band, $B^2\Sigma^+ - X^2\Sigma^+$ (0-1)) emission from natural and isotopically labelled benzoic acids as functions of distance above the sample surface are shown in Figures 3a and 3b, respectively. The emission profiles are normalized to the spatially integrated intensity. Only one representative delay time (2 μ s ICCD gate delay and 1.5 μ s gate width) is presented here. For each of the studied atomic and molecular species, the two benzoic acid samples, one with all carbons with natural isotopic abundance and the other with a ^{13}C -labelled terminus, had similar spatial emission profiles. Although the samples did not contain N, strong atomic N and molecular CN emission were observed due to nitrogen entrainment from air. Atomic N emission is from air breakdown whereas the CN molecules, which its reaction pathway of interest in this study, are formed from chemical reactions inside the plasma.

The effect of isotope substitution is further examined by measurement of plasma temperature. Because the plasma might not be in local thermodynamic equilibrium, plasma temperature can change depending on which temperature is being measured and from a particular thermometric species. For organic compounds, the popular atomic excitation temperature through Boltzmann plots is difficult to evaluate because there are not enough strong atomic emission lines with a wide range of excitation energies. In contrast, rotational temperature from strong molecular band (e.g., C_2 and CN) can be readily determined.

Figure 4a shows the spatial profiles of rotational temperatures derived from C₂ Swan (1–0) and CN violet (0–1) molecular bands. In general, the measured CN rotational temperatures were slightly higher than the C₂ rotational temperatures. For the same thermometric species, no difference within experimental uncertainty was found in the rotational temperatures from the two benzoic-acid samples. Spectra acquired at other delay time supported the same conclusion.

Figure 4b presents the half-width (FWHM) of the H α line against height in the plasma. Similar half-widths, within experimental uncertainties, were measured from benzoic acid with natural carbon-isotope abundance or ¹³C-labelled terminus. Results from Figures 3 and 4 support that isotopic substitution at the terminal carbon poses no significant effect on the characteristics of the laser induced plasma. Therefore, molecular formation mechanisms derived from the ¹³C-labelled sample are extendable to samples with natural isotopic abundance.

3.4 Isotopic patterns in C₂ and CN molecular emission and proposed mechanisms

The number-density ratios of ¹²C¹²C / ¹³C¹²C (i.e., $\alpha_{C_2} / \beta_{C_2}$) from the C₂ Swan (1–0) band as a function of height above the sample surface is shown in Figure 5a. For a particular delay time, the ¹²C¹²C / ¹³C¹²C ratios were uniform and no distinct spatial dependence was observed. In marked contrast, the ¹²C¹²C / ¹³C¹²C ratios rose steadily from ~ 3 to ~ 5 from delay time 0.6 μ s to 8 μ s. As discussed in Section 3.1, under the recombination mechanism Rx1 and the assumption that there is no preferential bond dissociation for benzoic acid in the plasma, the expected ¹²C¹²C / ¹³C¹²C ratio ($R^2 : 2R$) is 3. At 0.6 μ s delay (the earliest studied delay time), the experimental ¹²C¹²C / ¹³C¹²C ratio was essentially 3, supporting this proposed reaction

mechanism at very early delay time. The observation for the recombination mechanism agrees well with our previous study [33] in which a mixture of ^{12}C -benzoic acid and ^{13}C -amorphous carbon was used as the sample. Despite the fact that there were no ^{12}C - ^{13}C intermolecular bonds in the sample, strong $^{13}\text{C}^{12}\text{C}$ molecular emission was measured, presumably through a recombination pathway. However, results from our present experiment also clearly indicate that other mechanisms must be operative as the plasma evolves, because of the higher ratios at longer delay times (cf. Figure 5a).

Apart from recombination of free carbon atoms, direct release as a result of fragmentation from the sample has been proposed as an alternative source of C_2 molecules in a laser-induced plasma [8, 25, 33, 39]. Reports from different research groups shown that there is a direct link between the strength of C_2 emission and the molecular structure of the sample [8, 25, 39, 48-50]. The C_2 emission, in general, is comparatively weak for aliphatic organic compounds, significantly increases if the sample contains $\text{C}=\text{C}$ double bonds, and further increases for samples with aromatic rings [8, 25, 39, 48-50]. Because of the aromaticity of our sample, it is likely that some of the measured C_2 emission was native in origin. If some C_2 molecules are results of direct fragments from the aromatic ring, a higher-than-expected $^{12}\text{C}^{12}\text{C}$ population as seen in Figure 5a becomes logical and understandable because all carbon atoms in the ring are of natural abundance; the only ^{13}C -labelled carbon is at the terminus. The rise of $^{12}\text{C}^{12}\text{C} / ^{13}\text{C}^{12}\text{C}$ ratios at later delay time also supports this direct C_2 -desorption mechanism. As the plasma cools at longer delay times, atomization efficiency decreases as the plasma is less energetic to dissociate chemical bonds to form atoms; yet the plasma is hot enough to continue to desorb the sample through thermal means (e.g., thermal vaporization). Therefore, a larger fraction of the desorbed

sample survives as molecular fragments without undergoing atomization in the plasma plume. As a result, the contribution from recombination mechanism Rx1 becomes less to the overall C₂ formation, and the ¹²C¹²C population becomes higher than the values predicted by statistical distribution.

Figure 5b shows the ratio of the number densities of ¹²C¹⁴N / ¹³C¹⁴N (i.e., α_{CN} / β_{CN}) from the CN violet (0–1) band. Compared to experimental uncertainties, the ratios showed insignificant spatial dependence, and all CN ratios are upper-bounded by the stoichiometric ratio of 6. The ratios in C₂ and CN emission cannot be directly compared due to the symmetry of the ¹²C-¹²C molecule; for instance, if both C₂ and CN are formed by recombination reactions from atomic carbon with ¹²C / ¹³C ratio *R*, the isotopic patterns in ¹²C¹²C / ¹³C¹²C and ¹²CN / ¹³CN will be ½*R* and *R*, respectively (Section 3.1). It is possible to directly compare the isotopic patterns in C₂ and CN by conversion to atomic ¹²C / ¹³C ratio as derived from the molecular emission. In addition, because there was no clear spatial dependence on the isotopic patterns in both the C₂ and CN emission (cf. Figures 5a and 5b), all spectra at different vertical locations were summed and the resultant spectra were subject to the fitting procedure again for better precision. The results are presented in Figure 6.

The trends in the ¹²C / ¹³C ratios derived from C₂ and CN emission displayed opposite direction with increasing delay time (cf. Figure 6). The ¹²C / ¹³C ratios derived from C₂ emission demonstrated an unambiguous increase from the stoichiometric ratio of 6. In contrast, the ¹²C / ¹³C ratio derived from CN emission was similar, within experimental uncertainty, to the stoichiometric ratio at delay time 0.6 μs, but dropped to lower than 6 at longer delay times. The

opposite behavior between C₂ and CN provides several implications for their formation mechanisms. First, it is certain that the dissociation of carbon chemical bond is not complete and preferential bond breaking occurs, or otherwise the ¹²C / ¹³C ratios derived from the C₂ band should correlate with those from the CN band. Second, in contrast to some suggestions in the literature, the formation of CN through a four-center reaction of C₂ with nitrogen from air (i.e., Rx3a) [24-26, 51-53] can be ruled out. Figure 6 unambiguously refutes that C₂ is a key precursor for CN formation because of the lack of a correlation between the ¹²C / ¹³C isotopic ratios in C₂ and CN bands.

Preferential bond dissociation also could lead to a lower ¹²CN / ¹³CN ratio. In the above discussion, the higher ¹²C¹²C / ¹³C¹²C ratios are attributed to C₂ molecules derived from fragments directly from the aromatic ring; part of the ¹²C atoms are then trapped in these C₂ molecules without further dissociation. As a result, the fraction of carbon atoms that exist as ¹³C could be higher than the stoichiometric value, which offers an explanation for the lower ¹²CN / ¹³CN ratios.

4 Conclusion

Carbon isotope behavior (¹²C / ¹³C) in laser-induced plasmas was studied from C₂ and CN molecular emission with ¹³C-labelled benzoic acid as a model sample. Isotopic substitution in the sample induces negligible change in the plasma characteristics as the temporal and spatial behaviors of atomic (C, H, O, N) and molecular (CN and C₂) emission, and plasma fundamental properties (rotational temperatures and electron density) were similar. The results showed that the isotopic ratios (¹²C / ¹³C) derived from C₂ and CN exhibited opposite behaviors with respect

to delay time. The $^{12}\text{C} / ^{13}\text{C}$ ratio derived from the C_2 band was higher than its nominal value 6 whereas the ratio from the CN band was about or slightly below the nominal ratio for all measured delay times. These opposite trends indicate that dissociation of chemical bonds in the plasma is incomplete and selective. Some of the C_2 molecules exist directly from molecular fragments of the sample, preferably from the aromatic ring. In addition, the opposite behaviors from C_2 and CN unambiguously refute the mechanism that CN is formed from C_2 precursor. Formation of CN via atomic carbon (or species with a single carbon atom) is more viable.

The results also indicate that, for certain class of organic compounds, the analytical accuracy of LAMIS could be compromised by the formation mechanisms of the candidate species employed in isotope analysis. Understanding molecular formation mechanism, which in turn allows proper selection of experimental parameters, is crucial for better analytical performance in LAMIS. For instance, measurement at an early delay time for more complete sample dissociation and utilization of CN (over C_2) as the analytical molecular species for isotopic analysis of carbon, could mitigate the undesirable effects brought by mechanisms that give non-stoichiometric molecular species. The present study offers a better understanding of the laser-induced plasma chemistry, as well as the influence of molecular formation on the detection of isotopes by LAMIS.

Acknowledgment

The research was supported by the Office of Basic Energy Sciences, Chemical Science Division of the U.S. Department of Energy under contract number DE-AC02-05CH11231 at the Lawrence Berkeley National Laboratory. Meirong Dong and Jidong Lu acknowledge support from

National Natural Science Foundation of China (No. 51071069 and 51206055) and the Foundation of State Key Laboratory of Silicate Materials for Architectures (No. SYSJJ2014-01); we also thank Prof. Hongbin Ding from Dalin University of Technology for the helpful discussion.

References

1. Y.-I. Lee, K. Song, J. Sneddon, Laser-induced breakdown spectrometry, 1st ed., Nova Science Publishers Inc., Huntington, NY (2000).
2. D.M. Wong, A.A. Bol'shakov, R.E. Russo, Laser induced breakdown spectroscopy, in J.C. Lindon, G.E. Tranter, D.W. Koppenaal (eds), Encyclopedia of spectroscopy and spectrometry, 2nd ed., Academic Press, Oxford (2010) pp. 1281-1287.
3. R.E. Russo, T.W. Suen, A.A. Bol'shakov, J. Yoo, O. Sorkhabi, X. Mao, J. Gonzalez, D. Oropeza, V. Zorba, Laser plasma spectrochemistry, *J. Anal. At. Spectrom.* 26 (2011) 1596-1603.
4. J.P. Singh, S.N. Thakur (eds.), Laser-induced breakdown spectroscopy, 1st ed., Elsevier, Amsterdam (2007).
5. D.A. Cremers, L.J. Radziemski, Handbook of laser-induced breakdown spectroscopy, 1st ed., John Wiley & Sons, Chichester, U.K. (2006).
6. A.W. Miziolek, V. Palleschi, I. Schechter (eds), Laser-induced breakdown spectroscopy - fundamentals and applications, 1st ed., Cambridge University Press, Cambridge, UK. (2006).
7. R. Sattmann, I. Monch, H. Krause, R. Noll, S. Couris, A. Hatziapostolou, A. Mavromanolakis, C. Fotakis, E. Larrauri, R. Miguel, Laser-induced breakdown spectroscopy for polymer identification, *Appl. Spectrosc.* 52 (1998) 456-461.
8. S. Gregoire, M. Boudinet, F. Pelascini, F. Surma, V. Detalle, Y. Holl, Laser-induced breakdown spectroscopy for polymer identification, *Anal. Bioanal. Chem.* 400 (2011) 3331-3340.
9. J. Anzano, R.-J. Lasheras, B. Bonilla, J. Casas, Classification of polymers by determining of C₁ : C₂ : CN : H : N : O ratios by laser-induced plasma spectroscopy (LIPS), *Polymer Testing* 27 (2008) 705-710.

10. M. Baudelet, L. Guyon, J. Yu, J.P. Wolf, T. Amodeo, E. Frejafon, P. Laloi, Spectral signature of native CN bonds for bacterium detection and identification using femtosecond laser-induced breakdown spectroscopy, *Appl. Phys. Lett.* 88 (2006) 063901.
11. P. Lucena, A. Dona, L.M. Tobaría, J.J. Laserna, New challenges and insights in the detection and spectral identification of organic explosives by laser induced breakdown spectroscopy, *Spectrochim. Acta Part B* 66 (2011) 12-20.
12. C.G. Parigger, J.O. Hornkohl, A.M. Keszler, L. Nemes, Measurement and analysis of atomic and diatomic carbon spectra from laser ablation of graphite, *Appl. Opt.* 42 (2003) 6192-6198.
13. S. Acquaviva, M.L. De Giorgi, Study of kinetics of atomic carbon during laser ablation of graphite in nitrogen by time- and space-resolved emission spectroscopy, *Appl. Surf. Sci.* 186 (2002) 329-334.
14. S. Acquaviva, M.L. De Giorgi, High-resolution investigations of C₂ and CN optical emissions in laser-induced plasmas during graphite ablation, *J. Phys. B.* 35 (2002) 795-806.
15. G. Dinescu, E. Aldea, M.L. De Giorgi, A. Luches, A. Perrone, A. Zocco, Optical emission spectroscopy of molecular species in plasma induced by laser ablation of carbon in nitrogen, *Appl. Surf. Sci.* 127 (1998) 697-702.
16. M.R. Dong, X.L. Mao, J.J. Gonzalez, J.D. Lu, R.E. Russo, Time-resolved LIBS of atomic and molecular carbon from coal in air, argon and helium, *J. Anal. At. Spectrom.* 27 (2012) 2066-2075.
17. M. Capitelli, A. Casavola, G. Colonna, A. De Giacomo, Laser-induced plasma expansion: Theoretical and experimental aspects, *Spectrochim. Acta Part B* 59 (2004) 271-289.
18. Q. Lu, S.S. Mao, X. Mao, R.E. Russo, Theory analysis of wavelength dependence of laser-induced phase explosion of silicon, *J. Appl. Phys.* 104 (2008) 083301.
19. J. van Dijk, G.M.W. Kroesen, A. Bogaerts, Plasma modelling and numerical simulation, *J. Phys. D.* 42 (2009) 190301.
20. F. Vidal, S. Laville, T.W. Johnston, O. Barthelemy, M. Chaker, B. Le Drogoff, J. Margot, M. Sabsabi, Numerical simulations of ultrashort laser pulse ablation and plasma expansion in ambient air, *Spectrochim. Acta Part B* 56 (2001) 973-986.

21. L.V. Zhigilei, B.J. Garrison, Mechanisms of laser ablation from molecular dynamics simulations: Dependence on the initial temperature and pulse duration, *Appl. Phys. A* 69 (1999) S75-S80.
22. Q. Ma, P.J. Dagdigian, Kinetic model of atomic and molecular emissions in laser-induced breakdown spectroscopy of organic compounds, *Anal. Bioanal. Chem.* 400 (2011) 3193-3205.
23. V.I. Babushok, F.C. DeLucia, Jr., P.J. Dagdigian, J.L. Gottfried, C.A. Munson, M.J. Nusea, A.W. Miziolek, Kinetic modeling study of the laser-induced plasma plume of cyclotrimethylenetrinitramine (RDX), *Spectrochim. Acta Part B* 62 (2007) 1321-1328.
24. Z. Zelinger, M. Novotny, J. Bulir, J. Lancok, P. Kubat, M. Jelinek, Laser plasma plume kinetic spectroscopy of the nitrogen and carbon species, *Contrib. Plasma Phys.* 43 (2003) 426-432.
25. L. St-Onge, R. Sing, S. Bechard, M. Sabsabi, Carbon emissions following 1.064 μm laser ablation of graphite and organic samples in ambient air, *Appl. Phys. A* 69 (1999) S913-S916.
26. S. Abdelli-Messaci, T. Kerdja, A. Bendib, S. Malek, Emission study of C_2 and CN in laser-created carbon plasma under nitrogen environment, *J. Phys. D.* 35 (2002) 2772-2778.
27. Á. Fernández-Bravo, T. Delgado, P. Lucena, J.J. Laserna, Vibrational emission analysis of the CN molecules in laser-induced breakdown spectroscopy of organic compounds, *Spectrochim. Acta Part B* 89 (2013) 77-83.
28. R.E. Russo, A.A. Bol'shakov, X. Mao, C.P. McKay, D.L. Perry, O. Sorkhabi, Laser ablation molecular isotopic spectrometry, *Spectrochim. Acta Part B* 66 (2011) 99-104.
29. X. Mao, A.A. Bol'shakov, D.L. Perry, O. Sorkhabi, R.E. Russo, Laser ablation molecular isotopic spectrometry: Parameter influence on boron isotope measurements, *Spectrochim. Acta Part B* 66 (2011) 604-609.
30. X. Mao, A.A. Bol'shakov, I. Choi, C.P. McKay, D.L. Perry, O. Sorkhabi, R.E. Russo, Laser ablation molecular isotopic spectrometry: Strontium and its isotopes, *Spectrochim. Acta Part B* 66 (2011) 767-775.
31. A.A. Bol'shakov, M. Xianglei, C.P. McKay, R.E. Russo, Laser-ablation optical-cavity isotopic spectrometer for Mars rovers, *Proc. SPIE* 8385 (2012) 83850C.

32. A. Sarkar, X. Mao, G.C.Y. Chan, R.E. Russo, Laser ablation molecular isotopic spectrometry of water for ${}^2\text{D}/{}^1\text{H}$ ratio analysis, *Spectrochim. Acta Part B* 88 (2013) 46-53.
33. M.R. Dong, X.L. Mao, J.J. Gonzalez, J.D. Lu, R.E. Russo, Carbon isotope separation and molecular formation in laser-induced plasmas by laser ablation molecular isotopic spectrometry, *Anal. Chem.* 85 (2013) 2899-2906.
34. B. Yee, K.C. Hartig, P. Ko, J. McNutt, I. Jovanovic, Measurement of boron isotopic ratio with non-gated molecular spectroscopy of femtosecond laser-produced plasma, *Spectrochim. Acta Part B* 79-80 (2013) 72-76.
35. A. Sarkar, X. Mao, R.E. Russo, Advancing the analytical capabilities of laser ablation molecular isotopic spectrometry for boron isotopic analysis, *Spectrochim. Acta Part B* 92 (2014) 42-50.
36. R.E. Ferguson, On the origin of the electronically excited C_2^* radical in hydrocarbon flames, *J. Chem. Phys.* 23 (1955) 2085-2089.
37. A.A. Wyller, Vibrational temperatures of 5 carbon stars, *Astrophys. J.* 125 (1957) 177-194.
38. A. Stawikowski, J.L. Greenstein, Isotope ratio $\text{C}^{12}/\text{C}^{13}$ in comet, *Astrophys. J.* 140 (1964) 1280-1291.
39. S. Gregoire, V. Motto-Ros, Q.L. Ma, W.Q. Lei, X.C. Wang, F. Pelascini, F. Surma, V. Detalle, J. Yu, Correlation between native bonds in a polymeric material and molecular emissions from the laser-induced plasma observed with space and time resolved imaging, *Spectrochim. Acta Part B* 74-75 (2012) 31-37.
40. S. Acquaviva, Simulation of emission molecular spectra by a semi-automatic programme package: The case of C_2 and CN diatomic molecules emitting during laser ablation of a graphite target in nitrogen environment, *Spectrochim. Acta Part A* 60 (2004) 2079-2086.
41. S. Pellerin, K. Musiol, O. Motret, B. Pokrzywka, J. Chappelle, Application of the (0, 0) Swan band spectrum for temperature measurements, *J. Phys. D.* 29 (1996) 2850-2865.
42. G. Herzberg, *Molecular spectra and molecular structure: Spectra of diatomic molecules*, 2nd ed., Chapman and Hall, London (1950).
43. J.S.A. Brooke, P.F. Bernath, T.W. Schmidt, G.B. Bacskay, Line strengths and updated molecular constants for the C_2 Swan system, *J. Quant. Spectrosc. Radiat. Transf.* 124 (2013) 11-20.

44. R.S. Ram, S.P. Davis, L. Wallace, R. Engleman, D.R.T. Appadoo, P.F. Bernath, Fourier transform emission spectroscopy of the $B^2 S^+ - X^2 S^+$ system of CN, *J. Mol. Spectrosc.* 237 (2006) 225-231.
45. D.S. Pesic, B.R. Vujisic, D. Rakotoarijimy, S. Weniger, Band analysis of the Swan system ($d^3 \Pi_g - a^3 \Pi_u$) of $^{13}\text{C}_2$ and $^{12}\text{C}^{13}\text{C}$ molecules, *J. Mol. Spectrosc.* 100 (1983) 245-259.
46. R.S. Ram, P.F. Bernath, Fourier transform emission spectroscopy of the $B^2 S^+ - X^2 S^+$ (violet) system of $^{13}\text{C}^{14}\text{N}$, *Astrophysical Journal Supplement Series* 194 (2011) 34.
47. J.G. Phillips, Perturbations in Swan system of C_2 molecule, *J. Mol. Spectrosc.* 28 (1968) 233-242.
48. A. Portnov, S. Rosenwaks, I. Bar, Identification of organic compounds in ambient air via characteristic emission following laser ablation, *J. Lumin.* 102 (2003) 408-413.
49. A. Portnov, S. Rosenwaks, I. Bar, Emission following laser-induced breakdown spectroscopy of organic compounds in ambient air, *Appl. Opt.* 42 (2003) 2835-2842.
50. D.M. Wong, P.J. Dagdigan, Comparison of laser-induced breakdown spectra of organic compounds with irradiation at 1.5 and 1.064 μm , *Appl. Opt.* 47 (2008) G149-G157.
51. S. Wee, S.M. Park, Reactive laser ablation of graphite in a nitrogen atmosphere: Optical emission studies, *Opt. Comm.* 165 (1999) 199-205.
52. C. Vivien, J. Hermann, A. Perrone, C. Boulmer-Leborgne, A. Luches, A study of molecule formation during laser ablation of graphite in low-pressure nitrogen, *J. Phys. D.* 31 (1998) 1263-1272.
53. R.K. Thareja, R.K. Dwivedi, K. Ebihara, Interaction of ambient nitrogen gas and laser ablated carbon plume: Formation of CN, *Nucl. Instrum. Methods Phys. Res., Sect. B* 192 (2002) 301-310.

Figure Captions

- Figure 1 Spectrum of the $C_2 d^3\Pi_g - a^3\Pi_g (1-0)$ (Swan) band from ^{13}C -labelled benzoic acid. Due to the low abundance of ^{13}C in the sample ($^{12}C : ^{13}C = 6 : 1$), the expected intensity of the $^{13}C^{13}C$ band is $12 \times$ weaker than the $^{12}C^{13}C$ band.
- Figure 2 Comparison of experimental (symbols) and simulated spectra (red lines) for (a) $C_2 d^3\Pi_g - a^3\Pi_g (1-0)$ (Swan) band, and (b) $CN B^2\Sigma^+ - X^2\Sigma^+ (0-1)$ (violet) band. Two representative relative residuals (0.16 and 0.35 for fittings with good quality and near threshold, respectively) are presented.
- Figure 3 Spatial emission profiles of (a) atomic (C I 247.8 nm, H I 656.3 nm, O I 777.4 nm and N I 746.8 nm), and (b) molecular (C_2 and CN) species, from benzoic-acid samples with natural carbon-isotope abundance and a ^{13}C -labelled terminus. Gate delay and gate width were 2 μs and 1.5 μs , respectively. The emission was normalized to the area under the profile (i.e., spatially integrated emission). The error bars represent the standard deviations from four replicate measurements.
- Figure 4 Spatial profiles of (a) rotational temperatures derived from C_2 and CN molecular emission, and (b) measured line width (as FWHM) from the $H\alpha$ 656.3 nm line, from benzoic-acid samples with natural carbon-isotope abundance and a ^{13}C -labelled terminus. Gate delay and gate width were 2 μs and 1.5 μs , respectively. The error bars represent the standard deviations from four replicate measurements.
- Figure 5 Spatial profiles of number-density ratios of (a) $^{12}C^{12}C / ^{13}C^{12}C$, and (b) $^{12}CN / ^{13}CN$ at different delay time. The theoretical ratios assuming complete sample dissociation and molecular formation through recombination are 3 and 6 for C_2 and CN, respectively, and are marked accordingly with the dashed line. Data with solid

symbols represent the averaged values of individual spectrum fitting from the four replicates, and the associated error bars indicate the standard deviations. Data with hollow symbols are obtained by averaging the four spectra before the fitting procedure because the relative residuals through individual spectrum fitting were larger than the preset threshold (see text for discussion).

Figure 6 Temporal profiles of atomic $^{12}\text{C} / ^{13}\text{C}$ ratio as derived from the spatially averaged C_2 and CN molecular emission. The stoichiometric ratio in the sample is marked with the dashed line. The error bars represent the standard deviations from four replicate measurements.

Figure 1

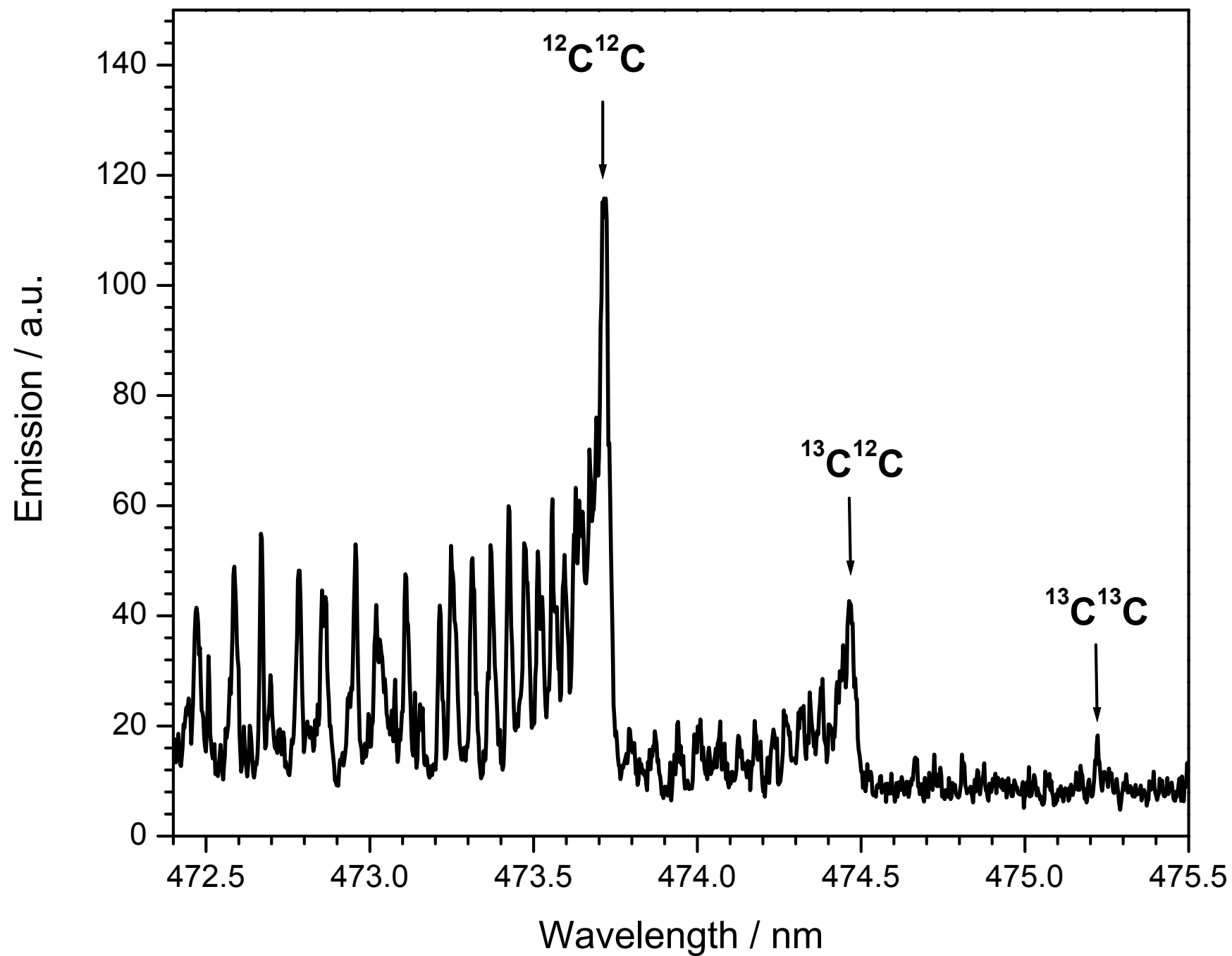


Figure 2a

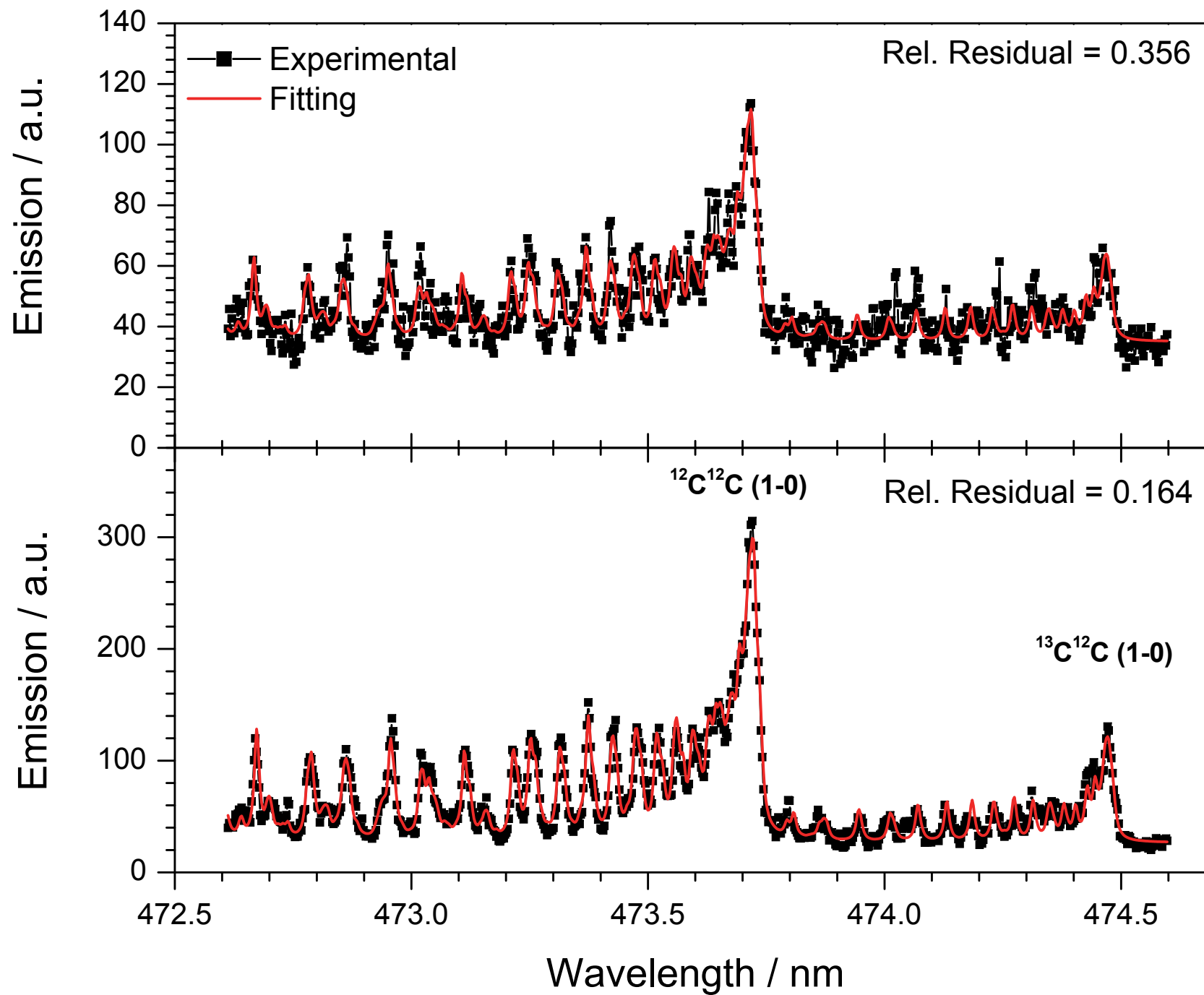


Figure 2b

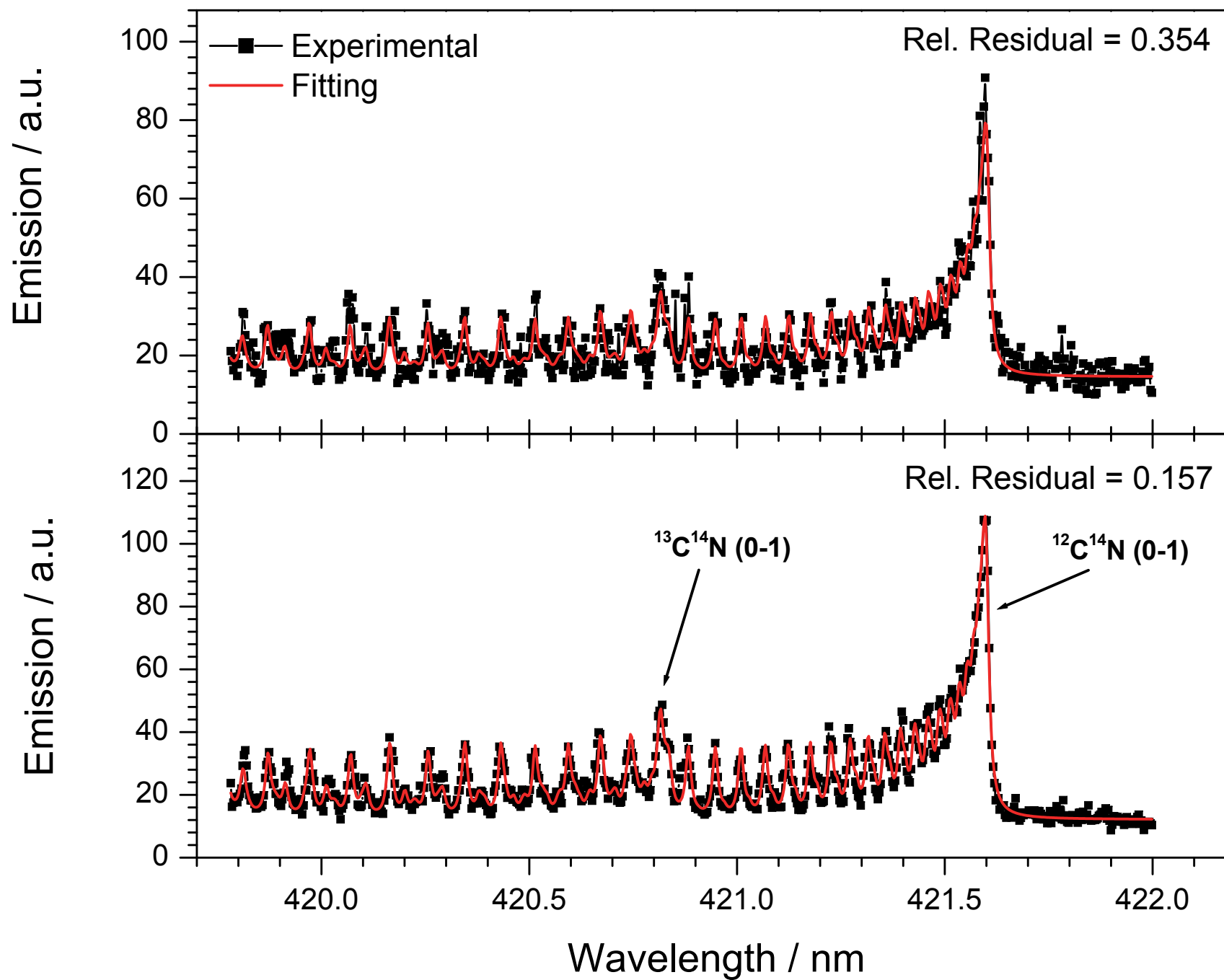


Figure 3a

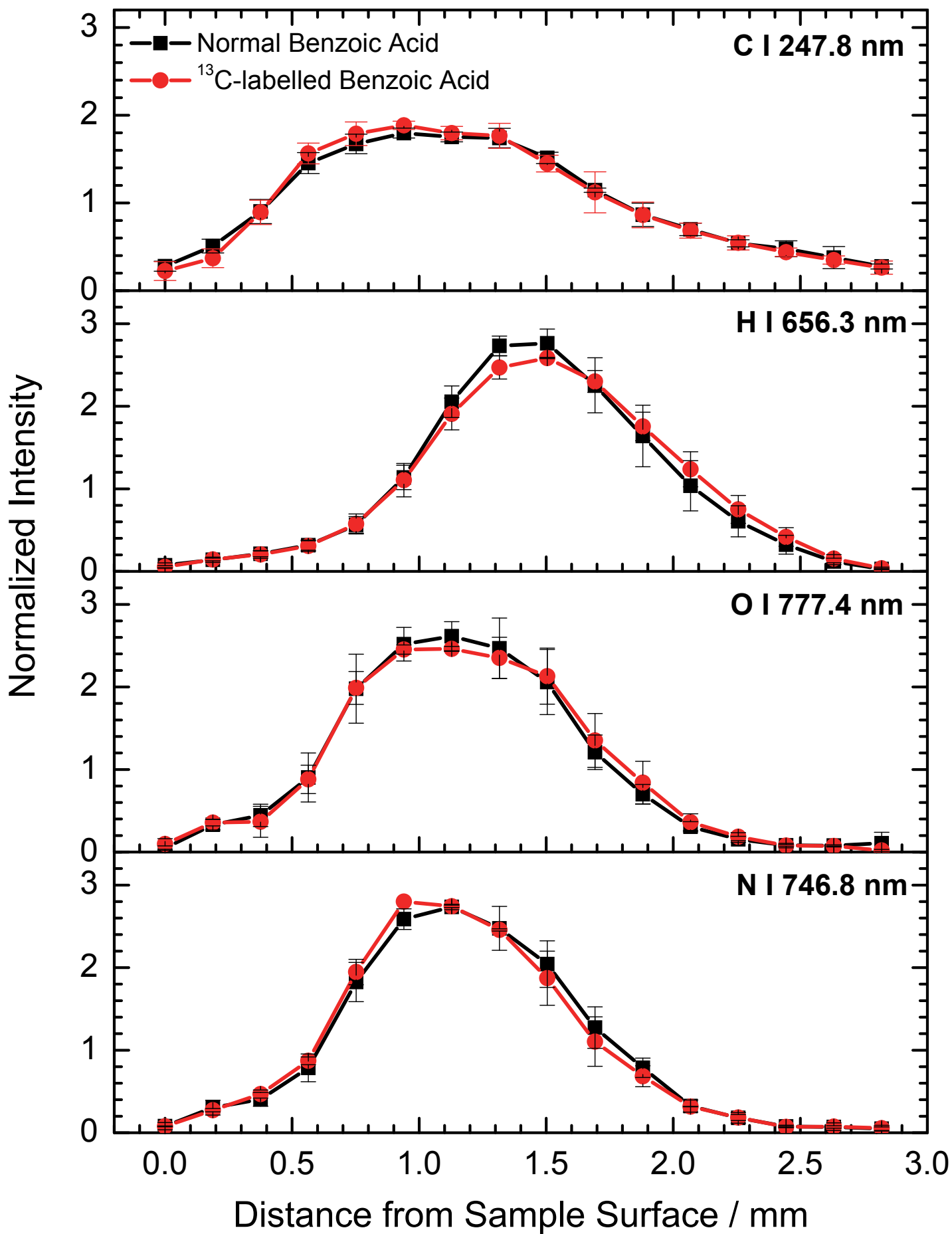


Figure 3b

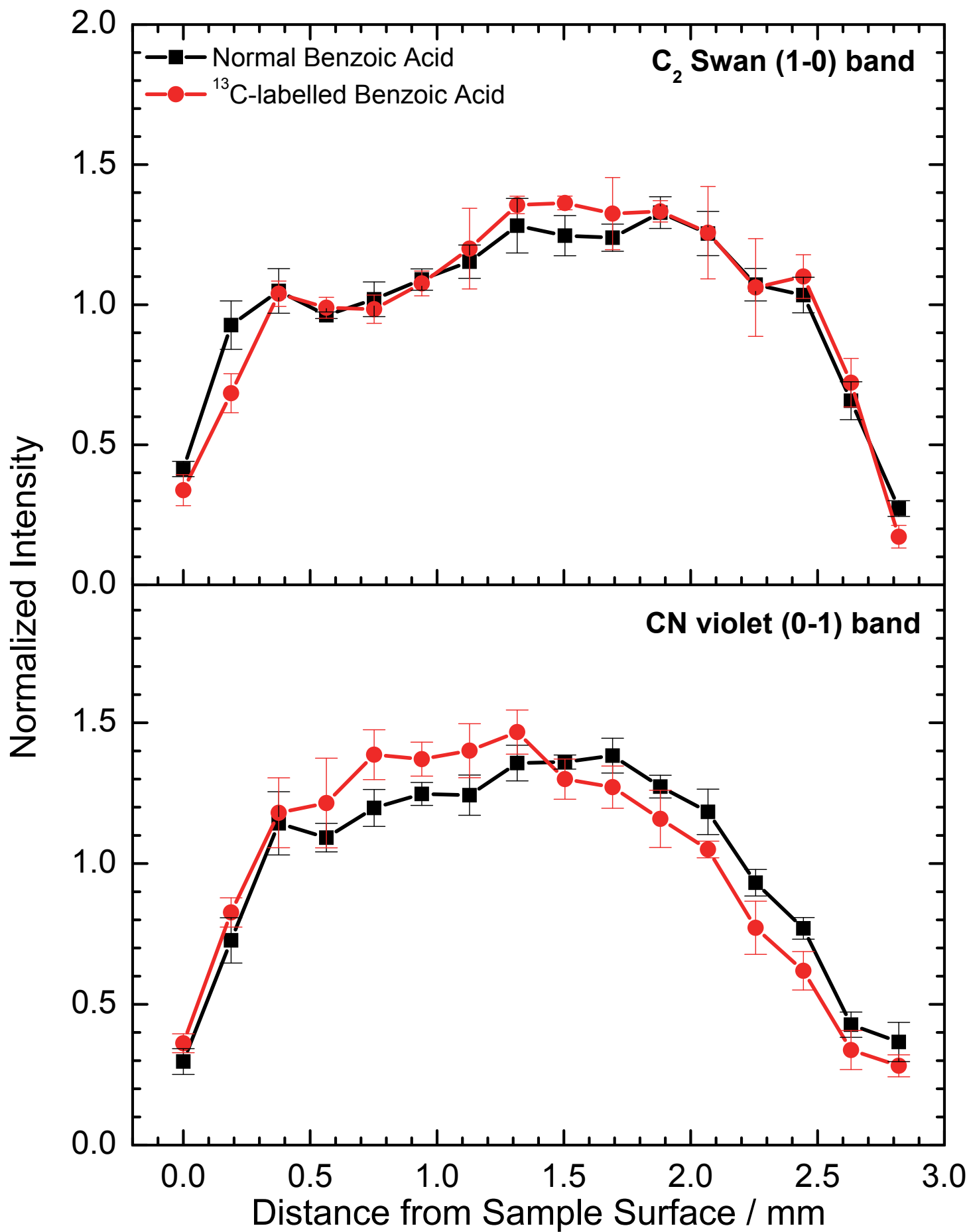


Figure 4a

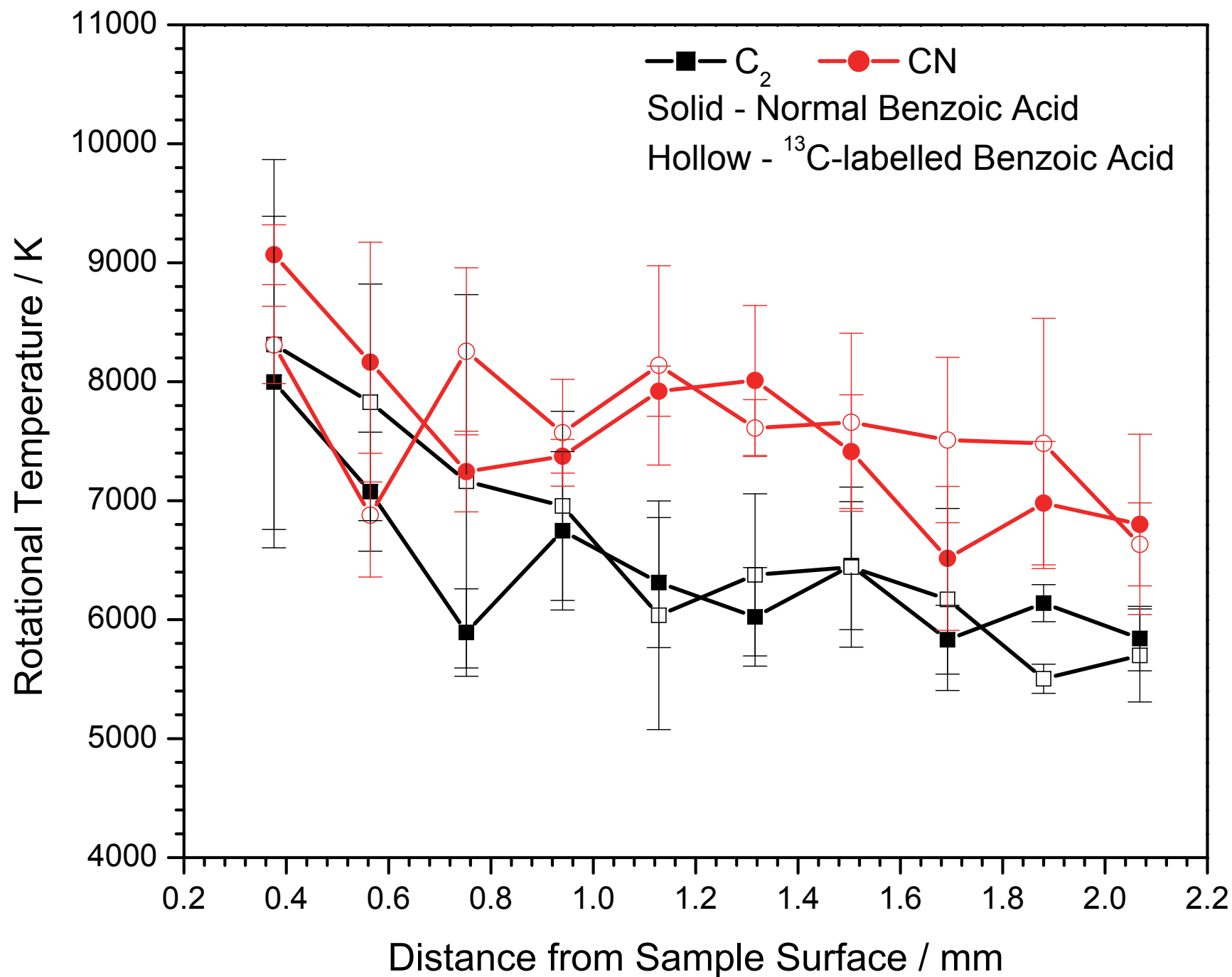


Figure 4b

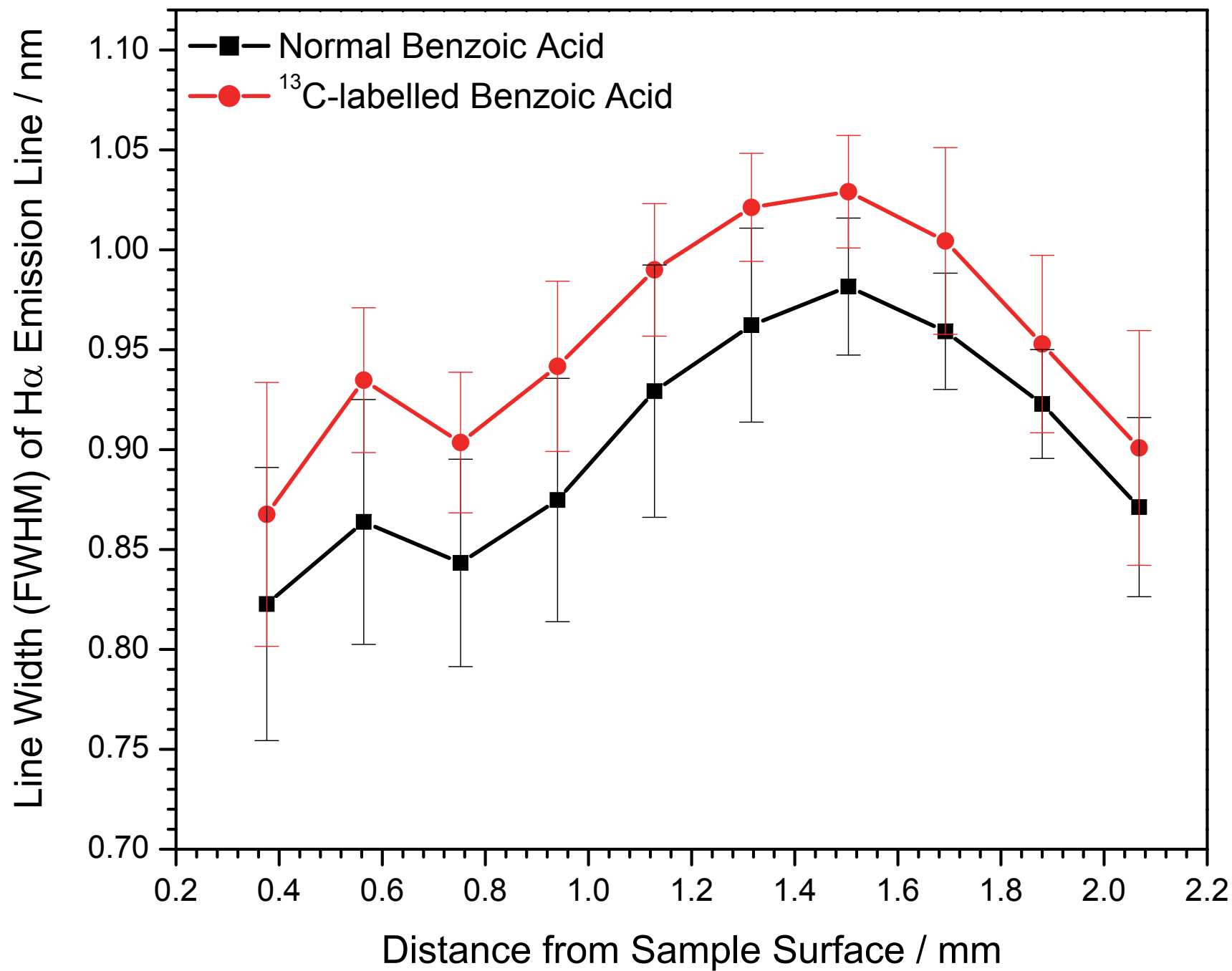


Figure 5a

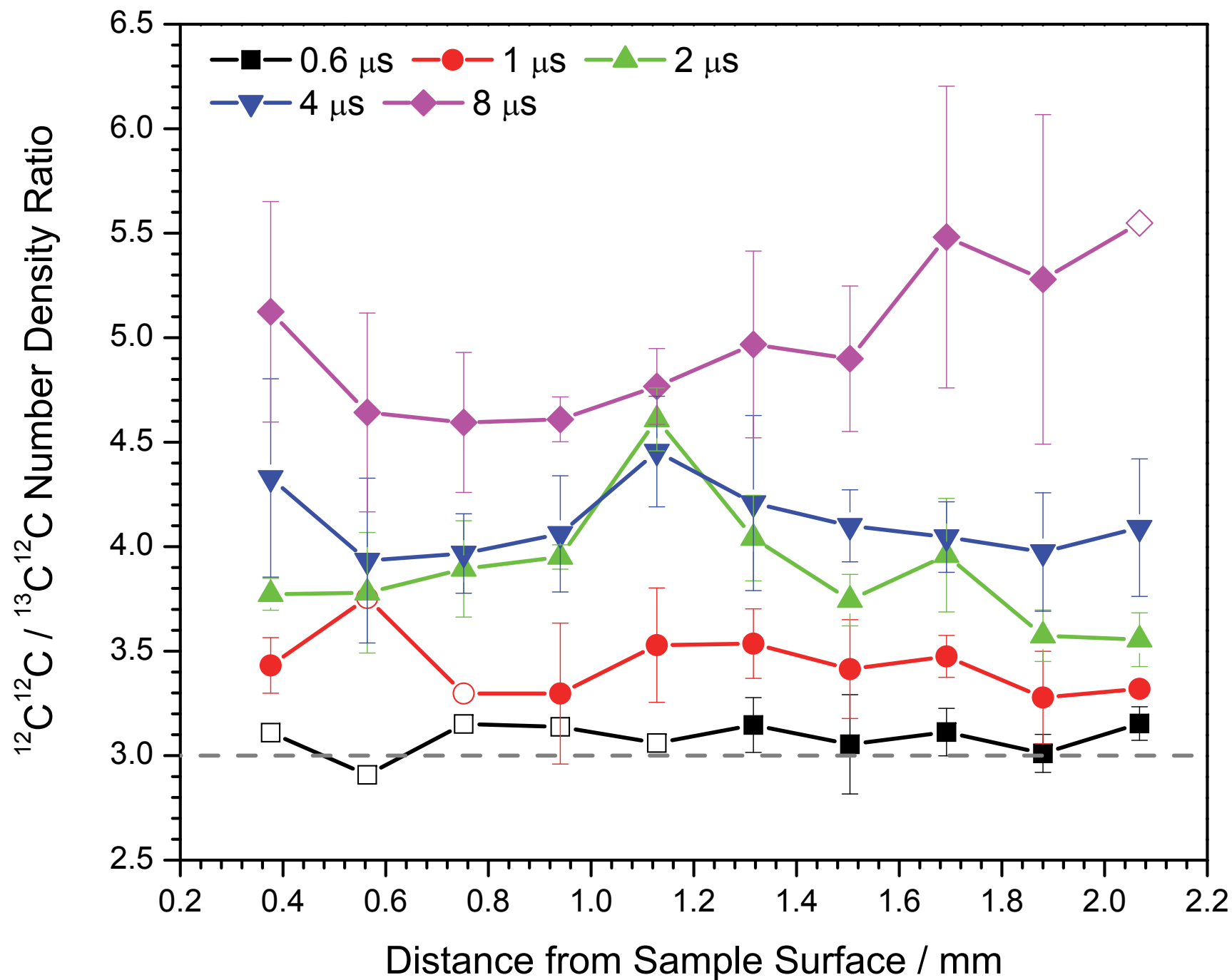


Figure 5b

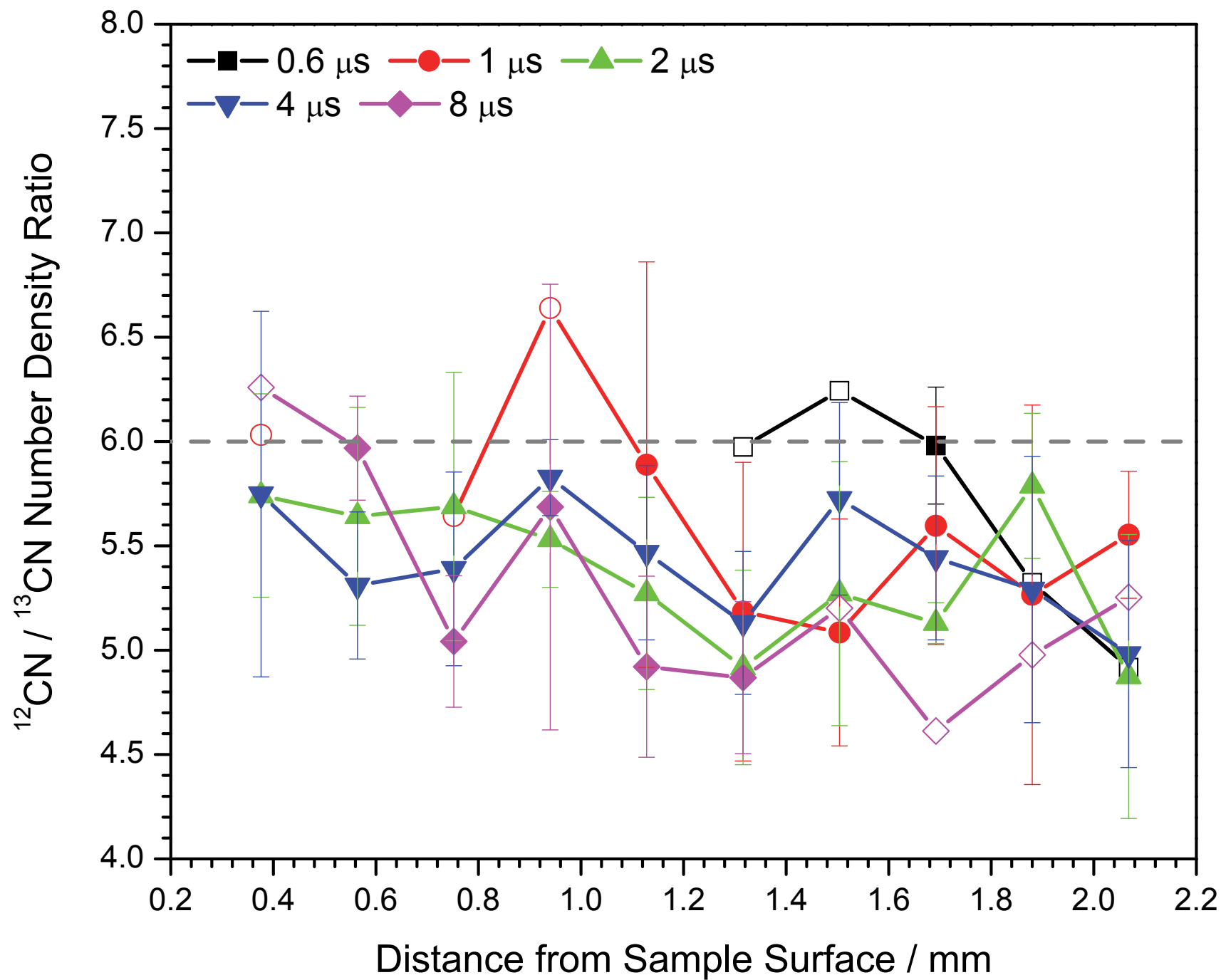


Figure 6

